electronics

Article

Surface Defect Detection of Steel Balls Based on Surface Full Expansion and Image Difference

Chen Li [1,2], Hongjun Ni [1,3,*], Hiroyuki Ukida [2], Jiaqiao Zhang [4], Bo Wang [1] and Shuaishuai Lv [1,*]

1 School of Mechanical Engineering, Nantong University, Nantong 226019, China; lchen@stmail.ntu.edu.cn (C.L.); 2410310012@stmail.ntu.edu.cn (B.W.)
2 Graduate School of Technology, Industrial and Social Sciences, Tokushima University, Tokushima 770-8506, Japan; ukida@tokushima-u.ac.jp
3 Institute of Intelligent Manufacturing, Nantong Institute of Technology, Nantong 226019, China
4 School of Mechanical Engineering, Southeast University, Nanjing 211189, China; 230218554@seu.edu.cn
* Correspondence: ni.hj@ntu.edu.cn (H.N.); lvshuaishuai@ntu.edu.cn (S.L.)

Abstract: The steel ball, as a key rolling element in mechanical equipment, directly affects the performance and service life of the bearing through its surface quality. Traditional methods for detecting surface defects on steel balls often face challenges in efficiency and stability. They struggle with three-dimensional surfaces and are easily affected by noise interference. This paper proposes a defect detection method for the steel ball surface based on Axial Cone mirror expansion and Improved Image Difference (ACID). The axial cone mirror unfolds the entire surface of the steel ball, allowing complete surface images to be obtained with just two captures. This simplifies the acquisition process and increases efficiency. The improved image difference method, combined with adaptive thresholding and adjacent frame difference techniques, effectively reduces noise interference. It enhances both the accuracy and robustness of defect detection. Frequent threshold adjustments and unstable detection, common in traditional methods, are avoided. Experimental results demonstrate that the ACID-based detection method surpasses traditional methods in terms of efficiency and accuracy. The improved method significantly reduces the missed detection rate. For example, the detection rates for cluster, scratch, and stain have increased from 86%, 80%, and 84% to 98%, 96%, and 98%, respectively. Moreover, the improved method reduces noise interference, avoids frequent threshold adjustments, simplifies the operation process, and shows higher stability and robustness in complex background conditions.

Keywords: steel ball surface; full surface expansion; image difference; defect detection

check for updates

Citation: Li, C.; Ni, H.; Ukida, H.; Zhang, J.; Wang, B.; Lv, S. Surface Defect Detection of Steel Balls Based on Surface Full Expansion and Image Difference. *Electronics* **2024**, *13*, 4484. https://doi.org/10.3390/electronics13224484

Academic Editor: Beiwen Li

Received: 21 October 2024
Revised: 11 November 2024
Accepted: 14 November 2024
Published: 15 November 2024

Copyright: © 2024 by the authors. Licensee MDPI, Basel, Switzerland. This article is an open access article distributed under the terms and conditions of the Creative Commons Attribution (CC BY) license (https://creativecommons.org/licenses/by/4.0/).

1. Introduction

As the rolling body of the bearing, the steel ball plays the role of transmitting force and carrying load [1], and its surface quality is directly related to the performance and service life of the bearing [2]. Surface defects, including clusters, scratches, and stains, can lead to premature fatigue flaking or fractures, thereby causing component failure during operation [3]. This compromises the normal functioning of the entire mechanical system and may result in serious industrial accidents. Therefore, detecting surface defects of steel balls efficiently and accurately holds significant practical importance in industry.

Currently, the three-dimensional curved structure of steel balls poses many challenges for surface image acquisition and defect detection. Existing detection methods are mainly based on the application of technologies such as photoelectric sensors, acoustic resonance, optical reflection, and machine vision. Daio Corporation (Ehime, Japan) [4] developed a surface defect detection machine for steel balls, which consists of a cylindrical roller and a helical roller set as the main part of the machine. To detect steel balls, the steel balls continuously change position within the detection machine, where photoelectric sensors collect data based on the principles of optical refraction and reflection. The collected data

are then analyzed by a computer to assess surface damage and evaluate the overall surface quality of the steel balls. However, this method suffers from low detection efficiency and struggles to ensure comprehensive and accurate detection. Japan's Tohoku Co., Ltd. [5] used the acoustic resonance principle to detect the surface defects of the steel ball and the integrity of the surface of the steel ball; the steel ball detection equipment uses air as a propagation medium, which is conducive to reducing the friction damage of the steel ball, but the method is not proposed to unfold the principle of the steel ball, and the use of the detection instrument is relatively inefficient in the detection. The Czech Republic's SOMET company [6], from 1961, began to produce the Aviko series of steel ball inspection systems. These systems use technologies such as photoelectric sensors, eddy currents, and vibration to automatically assess the surface quality of steel balls. The instrument is compact, easy to use, and offers high detection efficiency with a low leakage rate. However, as a contact-based detection method, it risks causing secondary damage to the steel balls and is costly, making it more suitable for high-precision inspections or batch sampling of steel balls. Japan's Amatsuji company independently developed a steel ball detection instrument using the meridian expansion principle of the steel ball surface defects detected, and then combined with laser technology to detect the ball surface damage minimum value of 35 μm [7], while acoustic technology [8] was used to detect the internal structure of the ball damage to the outer surface distance of 0.4 mm. Song Xiaoxia [9] et al. proposed a machine vision-based automatic detection method for surface defective tracks of steel balls. The whole sphere expansion method using six CCD (charge-coupled device) image sensors can accurately identify steel ball surface defects. The method proposed to use a feature extraction function to successfully classify the defects on the steel ball surface by calculating the RGB (Red, Green, Blue) values of the steel ball surface. Li Lin [10] et al. proposed a sphere expansion method based on dual image sensors for the surface defects of highly reflective spherical surfaces and miniature steel balls, and developed a miniature steel ball surface defect automatic detection and sorting instrument. The method is capable of detecting defects on micro steel balls with diameters ranging from 1.2 mm to 3.175 mm, with a detection speed of four grains per second and a leakage rate of only 0.02%. Song Yuhang [11] et al. developed a detector for the surface quality of steel balls based on the reflection streak detection method for highly reflective spherical surfaces, and designed the overall structure and control system of the detector. Papacharalampopoulos [12] et al. developed a surface quality assessment method based on deep learning and synthetic data, successfully detecting surface defects on solar reflectors during manufacturing and usage phases, and offering technical insights for defect detection on complex surfaces. Stavropoulos [13] et al. designed a vision-based real-time defect detection system for identifying defects in rubber composite parts, providing valuable reference for the development of real-time detection systems. Li [14] et al. proposed a surface defect identification method for steel balls based on an optimized support vector machine (SVM) model, significantly improving the accuracy and reliability of defect recognition for steel balls. These methods can work effectively under specific conditions, but there are still limitations in the comprehensive detection of surface defects on steel balls. Therefore, how to unfold the surface of a 3D steel ball into a 2D plane and then combine it with effective image processing techniques for defect detection has become one of the research focuses.

This paper proposes a defect detection method for steel ball surfaces based on Axial Cone mirror expansion and Improved Image Difference (ACID). It firstly converts the three-dimensional surface of the steel ball into a two-dimensional planar image through the surface expansion technique using the principle of specular reflection, allowing complete surface images to be obtained with just two captures. And then performs the difference processing between the normal image and the defective image, highlights the differences and minimizes the noise through the binarization technique, and finally identifies the defective region according to the adaptive threshold, so as to target different types of steel ball surface defects and to improve the detection efficiency.

2. Basic Theory

2.1. Principle of Full Expansion of Steel Ball Surface

The basic principle of full surface expansion involves mapping the three-dimensional surface of a steel sphere onto a two-dimensional plane, converting surface information into a planar image for comprehensive detection and analysis. Traditional methods of full surface expansion include spiral expansion, meridian expansion, and multiple shots using rollers and hollow spindles.

The spiral expansion method [15] achieves seamless coverage of the spherical surface by generating a spiral distribution of circular detection trajectories as the steel ball rotates around both the z-axis and x-axis. As shown in Figure 1, this method converts spherical points into spherical coordinates (r, α, β), and maps the polar angle α and azimuthal angle β to 2D plane coordinates (u, v), creating an unfolded image. While this approach systematically and continuously maps points from the spherical surface to a 2D plane to produce a seamless unfolded image, regions near the poles (where α approaches 0 or π) are compressed towards the image edges. This compression causes a sharp decline in image resolution in those areas, leading to significant information loss and difficulties in accurately detecting defects. Additionally, the polar coordinate transformation and mapping process involves complex mathematical calculations, which consume considerable computational resources and time.

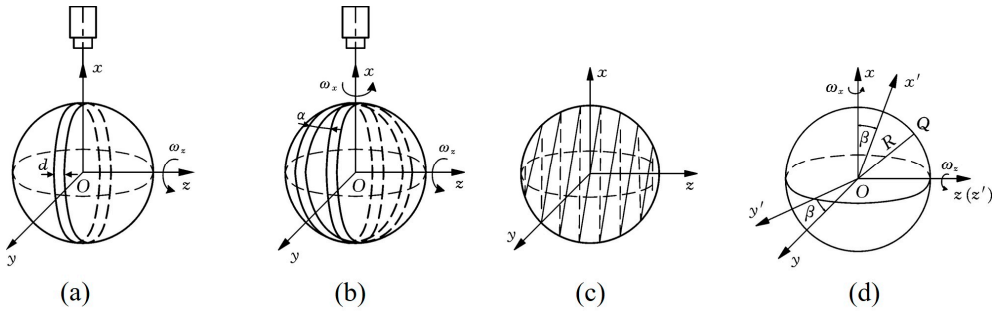


Figure 1. Spiral expansion process: (**a**) A circular surface, (**b**) Two circular surfaces, (**c**) Trajectory line, (**d**) Polar coordinate conversion.

The basic principle of the meridian expansion method is to use a specific rotating mechanism to make the steel ball make a rotating movement around its axis, and gradually unfold the spherical surface along the meridian direction in order to carry out a comprehensive inspection, which is a mature technology widely used in the unfolding of bearing steel balls, and is widely adopted in the field of steel ball manufacturing and inspection due to its high efficiency and accuracy. The Aviko unfolding system was used as an example [16], and its working principle is illustrated in Figure 2. The unfolding mechanism consists of a driving wheel, a compressor wheel, and a meridian wheel. The driving wheel uses friction to rotate the unfolding wheel and the steel ball, allowing for a full surface scan of the steel ball and ensuring that the sensor can accurately detect every position [17]. However, due to the asymmetrical design of the conical surface of the unfolding wheel, uneven forces are applied to the steel ball, which affects the uniformity of the unfolding process.

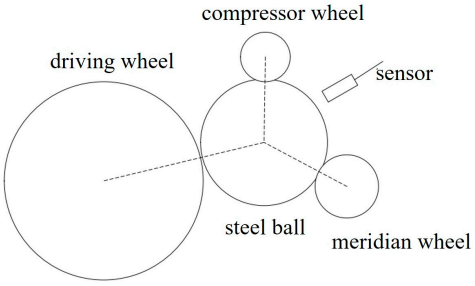


Figure 2. Basic principle of meridian expansion method for the Aviko system.

Kawabata et al. [18] proposed an expansion method for photographing the surface of a steel ball one at a time using a roller and a rotating shaft. In this method, a steel ball is placed on a rotating roller, and the ball is gradually rotated by the control of a rotating shaft to capture the image of the surface of the steel ball one by one, and the unfolding process is shown in Figure 3. The rotation of the roller ensures that the steel ball remains stable during the photographing process, and at the same time, by adjusting the angle of the rotary axis, it can cover different areas of the surface of the steel ball. In the shooting process, the entire surface of the steel ball is divided into multiple areas, one area is shot each time, and a complete image of the surface of the steel ball is finally obtained by rotating one after another, and the image shooting process is shown in Figure 4. Although this method can acquire information on the steel ball surface in a more comprehensive way, 32 images need to be taken for each ball to cover the whole surface, which is less efficient for detection. At the same time, due to the possible overlap between multiple images, it leads to the need to additionally consider how to deal with these overlapping areas during image processing to prevent data redundancy or errors.

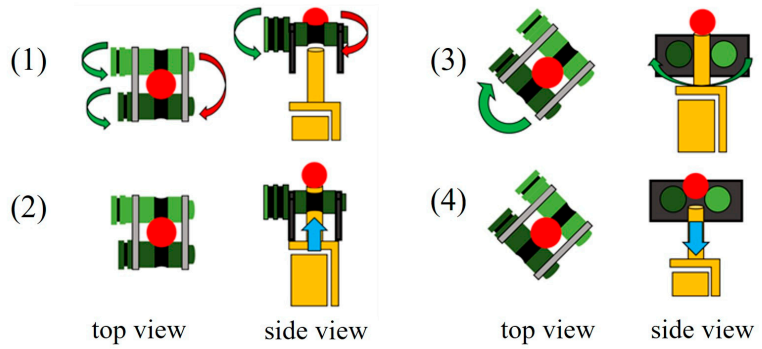


Figure 3. Expansion process using rollers.

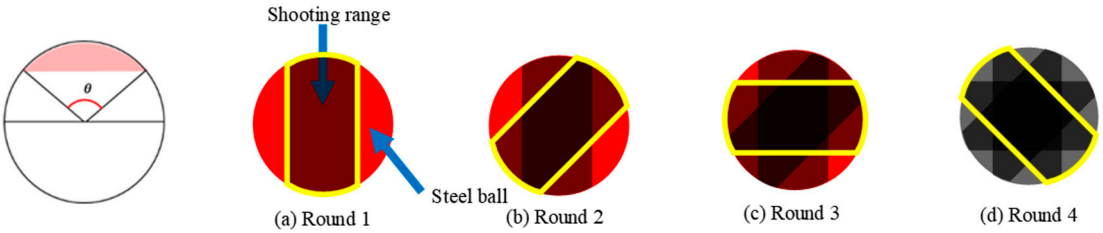


Figure 4. The process of taking images of the steel ball surface.

2.2. Basic Principle of Image Difference

2.2.1. Background Difference Method

Background difference [19] is a commonly used method in image processing and computer vision, and is mainly used to separate foreground targets from video sequences or image sequences. Its basic principle in the field of defect detection is to compare the input image with the background image to detect possible defective regions in the image, and its main process includes background modeling, foreground detection, thresholding, and post-processing. First, background modeling [20] is performed with the aim of obtaining a stable background image, then foreground detection is performed to obtain the difference image by calculating the difference between the defective image and the background image with the following formula:

$$D_t(x,y) = |I_t(x,y) - B(x,y)| \quad (1)$$

where "t" indicates the number of different frames in the defective image sequence, $I_t(x,y)$ is the pixel value of the defective image, $B(x,y)$ is the pixel value of the background image, and $D_t(x,y)$ is the difference image.

Thresholding is then performed and after the difference image $D_t(x,y)$ is calculated, the difference image is binarized by setting a threshold in order to separate the foreground targets [21]. The difference image is binarized by applying a threshold value T_b with the following formula:

$$F_t(x,y) = \begin{cases} 1, \ if \ D_t(x,y) \geq T_b \\ 0, \ otherwise \end{cases} \tag{2}$$

where $F_t(x,y)$ is the binarized foreground mask image, regions with a value of 1 are denoted as foreground targets (or defects), and regions with a value of 0 are denoted as background. Finally, post-processing is performed, which aims at using area threshold to remove small areas of noise points and connecting broken foreground regions, and commonly used operations include erosion, dilation, opening, and closing.

2.2.2. Adjacent Frame Difference Method

Adjacent frame difference [22] takes an image sequence as a target and selects two adjacent frames for pixel difference calculation to detect possible regions of change in the image. If the result of the difference operation is greater than or equal to a set threshold, the pixel is considered to be part of the target to be detected. If the result of the difference operation is less than the set threshold, the pixel is considered to be part of the background. This method is particularly suitable for detecting fast changes in moving objects or targets. Its calculation formula is as follows:

$$D_k(x,y) = |I_k(x,y) - I_{k-1}(x,y)| \tag{3}$$

where $D_k(x,y)$ denotes the difference result between the kth frame image $I_k(x,y)$ and the (k $-$ 1)th frame image $I_{k-1}(x,y)$.

In order to distinguish the foreground changes from the noise in the background, the difference image $D_k(x,y)$ needs to be thresholded. A threshold T_b is set to binarize the difference image with the following formula:

$$F_k(x,y) = \begin{cases} 1, \ if \ D_k(x,y) \geq T_b \\ 0, \ otherwise \end{cases} \tag{4}$$

If $F_k(x,y) = 1$, it indicates that the pixel is part of the foreground target region to be detected; if $F_k(x,y) = 0$, the pixel is part of the background region. Finally, the binarized image resulting from the adjacent frame difference method is subjected to morphological operations and connectivity domain analysis to remove small, isolated regions in order to reduce false detections.

2.2.3. Adaptive Threshold Method

In the image difference method, manually setting or calculating the threshold is the key step [23], but the traditional method of obtaining the threshold is to set it manually based on practical experience, which is highly subjective. Another method is the adaptive threshold technique [24], including the Otsu method [25] and the mean value method [26]. The Otsu method is an adaptive threshold method based on the global pixel grey level histogram, which determines the optimal threshold by maximizing the inter-class variance, thus dividing the image into foreground and background parts. The mean value method dynamically determines the threshold value by calculating the average of the pixel values in the image or its local blocks to classify pixels as foreground or background. Although the adaptive threshold method avoids the problem of relying on subjective experience, it does not handle well in the face of low noise.

3. The ACID-Based Steel Ball Surface Defect Detection Method

3.1. Full Expansion of Steel Ball Surface Based on Axial Cone Mirror

The specular reflection expansion method [27] is a steel ball surface unfolding method based on the optical reflection principle, by placing the ball on a plane consisting of multiple mirrors, the full surface unfolding image of the ball is finally obtained on the plane by simulating the reflection of light rays from the surface of the ball to the mirrors. In this study, the axial cone mirror is used for the full expansion of the surface of the steel ball, and only two shots are needed to obtain the complete surface image, which greatly improves the efficiency of the full expansion of the surface of the steel ball. As shown in Figure 5, the top and surrounding images of the steel ball can be acquired at one time by adding an axial cone mirror without changing the position of the ball several times to acquire the complete surface image, which greatly improves the efficiency of acquiring the full surface image of the steel ball. As shown in Figure 6, the detection range is from 0 degrees to 120 degrees from the top black area to the bottom green area. The axial cone mirror is a part of an inverted cone with a mirrored interior. By placing the steel ball in the center of the axial cone mirror and photographing it from the top, it is possible to directly photograph the upper part of the ball and all sides of the ball on the axial cone mirror without having to change the orientation of the ball and take multiple shots. In this way, an image of the top of the steel ball and the surrounding area can be obtained in a single shot, and an image of the bottom of the steel ball can be obtained by rotating the steel ball through the drum in a horizontal direction once, and then taking another shot. Thus, a complete image of the surface of the steel ball can be obtained in only two shots.

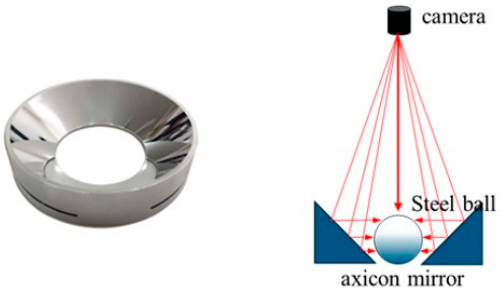


Figure 5. Axial cone mirror and principle of expansion.

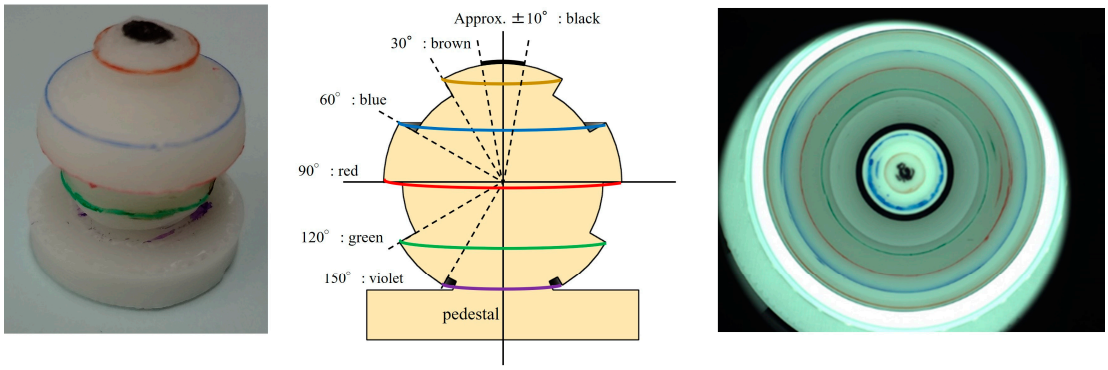


Figure 6. A model to check the area of angle that can be captured.

The surface expansion method utilizing an axial cone mirror offers several key benefits the following: (1) Global Feature Preservation: this technique maintains the integrity of the steel ball's surface characteristics through mirror reflection, thereby minimizing distortion in polar and boundary areas. (2) Boundary continuity: the specular reflection expansion method can make the boundary of the unfolding map more continuous and smooth by cleverly designing the arrangement of mirrors and reflection angles, avoiding the common edge discontinuity problem in the traditional method. (3) visual realism: the use of specular

reflection can better simulate the reflection characteristics of the surface of the ball, so that the unfolded map has a higher sense of visual realism, which is especially suitable for the field of graphics and visual computing.

3.2. Surface Defect Detection of Steel Balls Based on Improved Image Difference

The selection of threshold in the difference method is too dependent on subjective experience, and the adjacent frame difference method is more suitable for dynamic real-time defect detection, so we combine the background difference method and the adjacent frame difference method, and propose an improved image difference method for defect detection on the surface of steel balls. The method can overcome the subjective influence of threshold setting, and at the same time can minimize the interference of noise and highlight the defective regions.

This method assumes that the normal image changes slightly each time it is taken, so a stable background model needs to be produced first. The algorithmic flow of the method is divided into two parts: (a) using the adjacent frame difference method to produce a stable background model; and (b) using the adaptive threshold method for defect detection. The flowchart of the improved algorithm is shown in Figure 7.

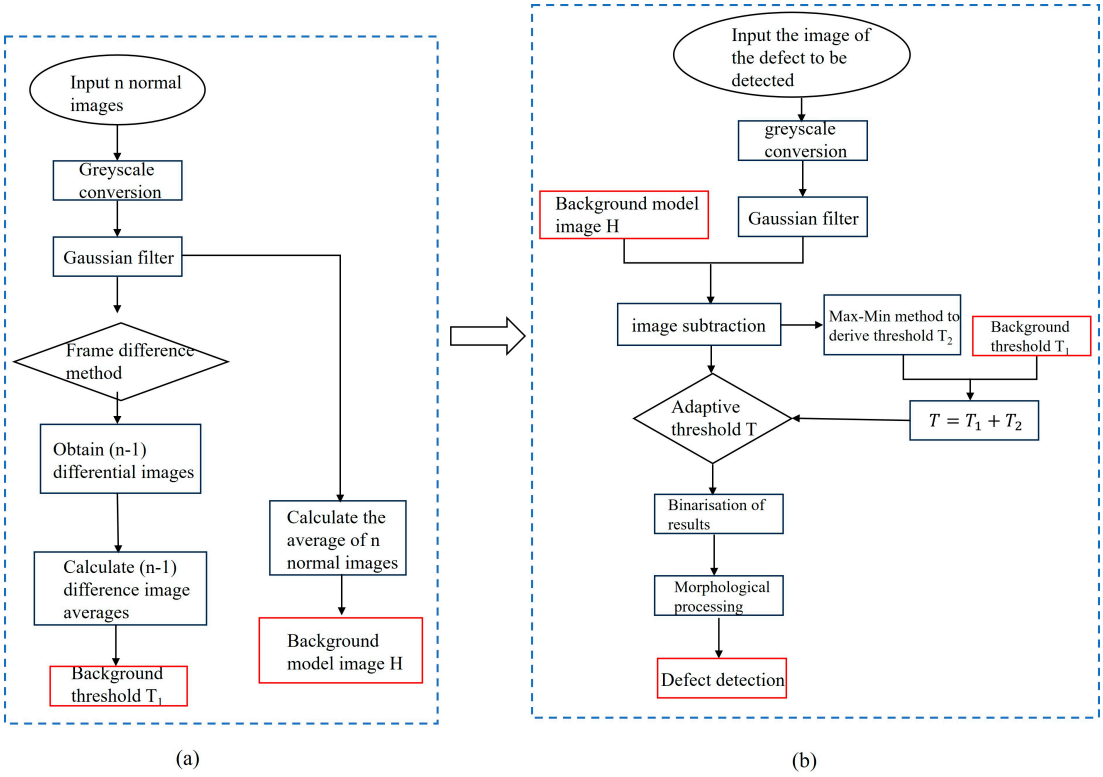


Figure 7. Flowchart of the improved algorithm: (**a**) Background modeling, (**b**) Acquisition of adaptive threshold and defect detection.

(a) Background modeling

Step 1: obtain n normal images of the steel ball surface using the improved steel ball surface expansion method;

Step 2: convert the n normal images into grayscale images and perform the Gaussian smooth filter;

Step 3: compute the average value of the n grayscale images to obtain the background model image H;

Step 4: For the n grayscale images, apply the adjacent frame difference method to obtain the $n - 1$ background difference images, and then compute their average value to obtain the background threshold image T_1. Then, calculate their average value to obtain

the background threshold T_1, and the calculation formula is shown in Equation (5). The final background model image and background threshold are generated for subsequent defect detection.

$$T_1 = \frac{1}{w \cdot h} \sum_{x=0}^{w-1} \sum_{y=0}^{h-1} \left\{ \frac{1}{k-1} \sum_{k=2}^{n} D_k(x,y) \right\} \tag{5}$$

(b) Acquisition of adaptive threshold and defect detection

Step 1: convert the defect to be detected into a grayscale image and use the Gaussian smooth filter to obtain a low-noise grey scale image;

Step 2: calculate the difference between the defect image to be detected and the background model image H, and obtain a difference image;

Step 3: by analyzing the range of pixel values in the difference image, use the max-min averaging method to calculate a new threshold value T_2, which helps to distinguish between the foreground and the background;

Step 4: adaptive threshold T is obtained by adding the background threshold T_1 and the threshold T_2;

Step 5: the difference image is binarized using the adaptive threshold T to obtain a binarized image;

Step 6: Morphological processing is performed on the binarized image, first applying an opening operation to remove noise, followed by a closing operation to enhance the continuity of defect regions. Regions with a value of 255 are identified as defects. The calculations are shown in Equations (6) and (7).

$$T_2 = \frac{Max + Min}{2} \tag{6}$$

$$T = T_1 + T_2 \tag{7}$$

4. Experimental Results and Analysis

4.1. Steel Ball Surface Image Acquisition Platform Construction

This experiment builds a steel ball surface image acquisition platform, which mainly consists of an imaging system, an illumination system, a mechanical transmission and surface expansion system, an optical isolation system, and a PC.

(1) Imaging system: The system is primarily composed of a camera and a lens. Telecentric lenses are often used in visual inspection because they can capture distortion-free images, but they have the disadvantage of a narrower shooting range. In this study, a normal lens is used to capture both the surface of the ball and the surface of the axial lens. Figure 8 shows the difference between the normal lens and the telecentric lens.

(2) Illumination system: The platform is equipped with two types of lighting: dome lighting and coaxial lighting. Dome lighting illuminates the entire surface of the dome uniformly, but it is supplemented by coaxial lighting to illuminate the upper area of the dome due to shadows on the top caused by the holes in the camera position. The combination of the two illumination methods ensures that the surface of the steel ball is uniformly and fully illuminated, avoiding the detection of blind spots due to uneven lighting. Figure 9 shows the results of the different illumination methods: when only the dome lighting is used (Figure 9a), the upper part of the steel ball is dark; when only the coaxial lighting is used (Figure 9b), only the upper part is illuminated; and when the two types of illumination are used at the same time (Figure 9c), the entire steel ball is illuminated.

(3) Mechanical transmission and surface expansion system: The mechanical transmission component mainly consists of a lifting mechanism and a vertical moving slider, which allows precise adjustment of the distance between the steel ball and the lens, ensuring optimal image focus and clarity. Additionally, the equipment's position can be flexibly adjusted, enabling effective detection of steel balls of varying sizes. The surface expansion system comprises an axicon mirror and a hollow turntable. Through the

optical reflection of the axicon mirror, the three-dimensional curved surface of the steel ball is transformed into a two-dimensional plane.

(4) Optical Isolation System: The optical isolation system is primarily composed of a detection black box and a light source adjustment device. Due to the high reflectivity of the steel ball's surface, the black box encloses the platform to prevent interference from external light sources. By adjusting the intensity of the light source, the reflection spots on the steel ball's surface are minimized, thereby enhancing image quality and improving the accuracy of detection [28].

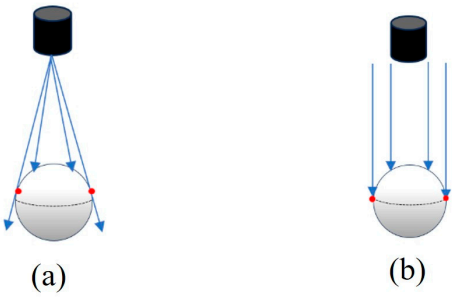


Figure 8. Difference between normal and telecentric lenses: (**a**) normal lens, (**b**) telecentric lens.

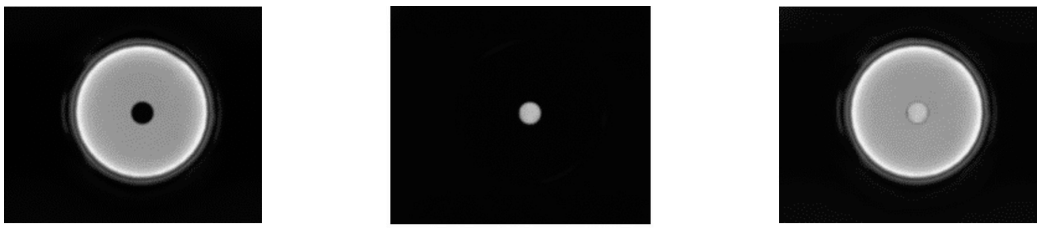


Figure 9. Shooting results of different lighting methods: (**a**) Dome lighting only, (**b**) Coaxial lighting only, (**c**) Simultaneous use of two types of lighting.

The material of the steel ball to be detected is high-carbon chrome-bearing steel with a diameter of 12.7 mm. The hardware device is controlled by IAI toolbox software (https://www.intelligentactuator.com/iai-software/), and the overall algorithm is implemented by Visual Studio 2022 software, which can be performed by an ordinary PC to avoid the waste of computing resources. Figure 10 shows the composition of the detection device and the steel ball to be detected. Figure 11 presents the defect detection platform for steel balls set up in the laboratory environment. Table 1 lists the names and models of the key components of the detection device.

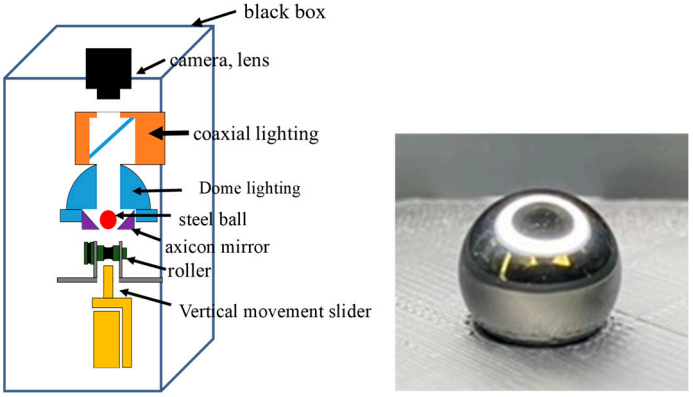


Figure 10. Components of the detection device and steel ball to be detected.

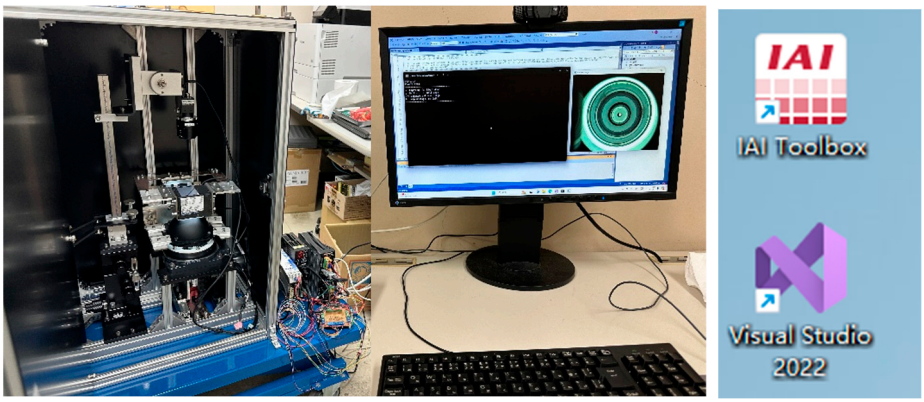


Figure 11. Steel ball defect detection platform.

Table 1. Components and Models.

Name	Model	Source
Camera	STC-MCS500U3V	Omron Sentech (Kyoto, Japan)
Lens	SV3514H	VS Technology (Kyoto, Japan)
Coaxial lighting	FA OPX-S50W2	Optex FA (Kyoto, Japan)
Dome lighting	FA OPD-S100W	Optex FA (Kyoto, Japan)
Axial cone mirror	Customization	VS Technology (Kyoto, Japan)
Lifting mechanism	EC-T3L-30-1-1-CJL	IAI (Shizuoka, Japan)
Vertical moving slider	EC-TW4L-50-S1-B	IAI (Shizuoka, Japan)

4.2. Steel Ball Surface Image Acquisition

Utilizing the high-precision image acquisition platform, we successfully obtained 200 high-resolution images of steel ball surfaces, focusing on three typical defects: clusters, scratches, and stains.

During the image acquisition process, the axial cone mirror unfolding technique is utilized to obtain a complete surface image of the steel ball in only two shots, achieving a full surface unfolding. This full unfolding converts a 3D surface into a 2D plane image through optical reflection, ensuring that the entire surface of the steel sphere is captured in its entirety and without omission. The combination of a telecentric lens and an optimized illumination system ensures that the image remains high resolution and low distortion during the unfolding of the surface of the steel ball, especially in the edge areas where details remain sharp. This seamless full-surface unfolding design allows for full detection of defects throughout the entire sphere, successfully realizing the full unfolding of the steel ball surface. Figure 12 shows an image of the unfolded surface of a steel ball, and Figure 13 shows samples of the captured image, which include a normal steel ball surface image and three types of defect images.



Figure 12. Image of the surface of the unfolded steel ball.

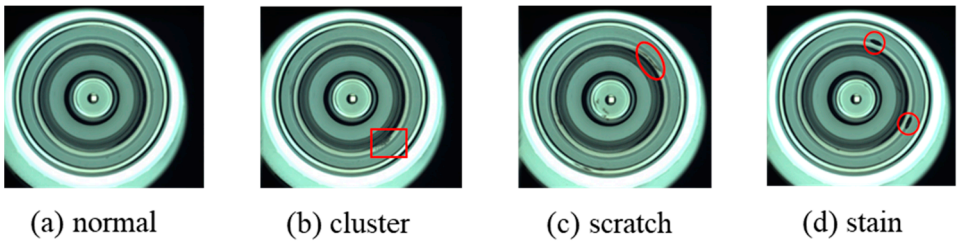


Figure 13. Normal and defective images.

4.3. Detection of Surface Defects on Steel Balls

Taking cluster defect as an example, a comparison was made between the improved image difference method and the traditional background subtraction method [29].

4.3.1. Defect Detection Based on Traditional Background Difference

(1) Comparison of two normal images

Step 1: (i) subtract normal image (a) from normal image (b); (ii) set the binarization thresholds to 30, 20, and 10, respectively; the results are shown in Figure 14; and(iii) find the appropriate binarization threshold to minimize the difference between the two normal images and prepare for the subsequent detection of defective regions.

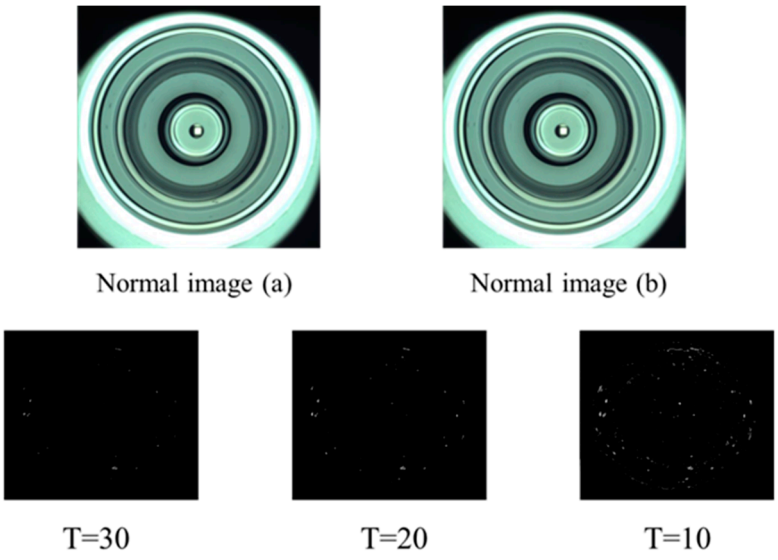
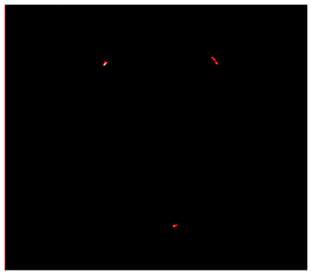
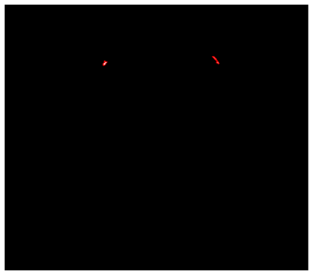
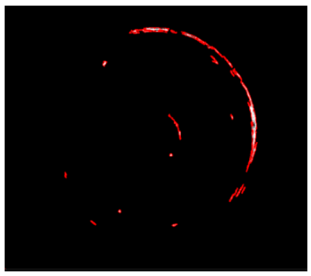
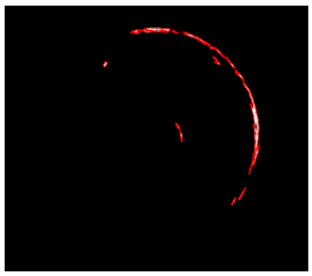
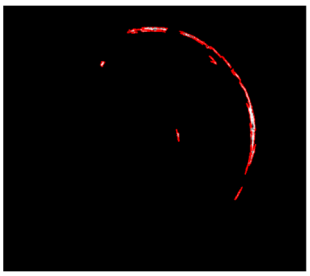
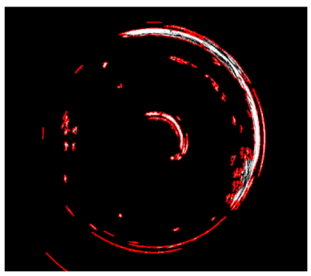
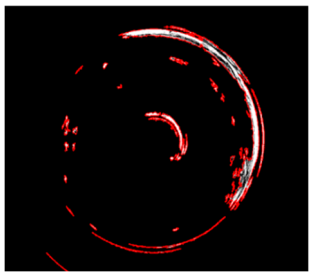
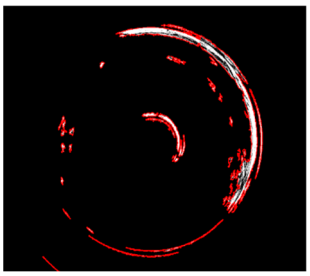


Figure 14. Binarization results of normal image after subtraction with thresholds set to 30, 20, and 10, respectively.

Step 2: (i) set the area thresholds to 100, 150, and 200, respectively, and compare the binarization results of the differences between the normal steel ball images obtained in step 1 to minimize the noise region; (ii) as shown in Table 2, when the binarization threshold is set to 30, the results for area thresholds of 100, 150, and 200 are displayed in (1), (2), and (3), respectively; (iii) when the binarization threshold is set to 20, the results for area thresholds of 100, 150, and 200 are displayed in (4), (5), and (6), respectively; and finally (iv) when the binarization threshold is set to 10, the results for area thresholds of 100, 150, and 200 are displayed in (7), (8), and (9), respectively.

Table 2. Results corresponding to different binarization thresholds and area thresholds.

Binarization threshold	Area Threshold: 100	Area Threshold: 150	Area Threshold: 200
30	 (1)	 (2)	 (3)
20	 (4)	 (5)	 (6)
10	 (7)	 (8)	 (9)

According to the above results, the difference between normal steel balls is minimized when the binarization threshold is set to 30, while the noise can be minimized when the area threshold is set to 200.

(2) Comparison of normal image and defective image

Step 1: (i) subtract the normal image from the defective image; (ii) set the binarization thresholds to 30, 20, and 10, respectively; and (iii) compare these results with the previous results, and the results are shown in Figure 15.

Step 2: (i) distinguish between "noise area" and "defective area", and divide the defective area by setting the area threshold, which is set to 100, 150, and 200, respectively; (ii) as shown in Table 3, when the binarization threshold is set to 30, the results for area thresholds of 100, 150, and 200 are displayed in (10), (11), and (12), respectively; (iii) when the binarization threshold is set to 20, the results for area thresholds of 100, 150, and 200 are displayed in (13), (14), and (15), respectively; and (iv) when the binarization threshold is set to 10, the results for area thresholds of 100, 150, and 200 are displayed in (16), (17), and (18), respectively.

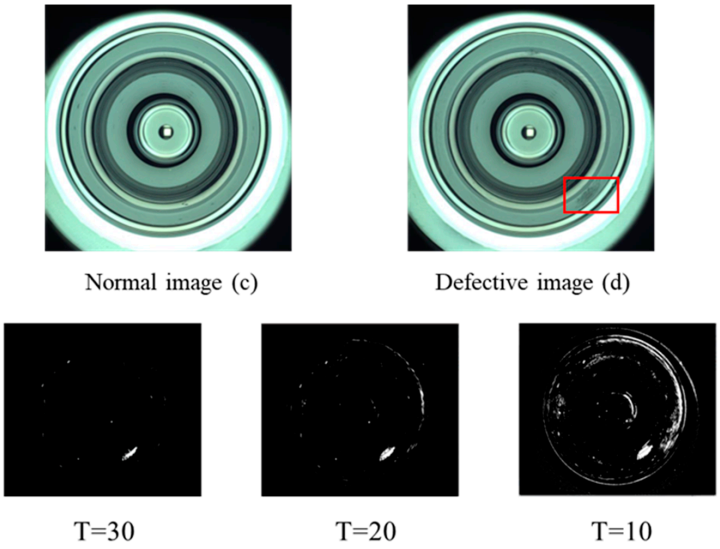


Figure 15. Binarization results of normal and defective images after subtraction with thresholds set to 30, 20, and 10, respectively.

Table 3. Defect segmentation results corresponding to different binarization thresholds and area thresholds.

Binarization threshold	Area Threshold: 100	Area Threshold: 150	Area Threshold: 200
30	(10)	(11)	(12)
20	(13)	(14)	(15)
10	(16)	(17)	(18)

According to the above results, for the scratch defects on the surface of the steel ball, after binarizing the defect image and subtracting the defect image from the original image, when the binarization threshold is set to 30, the main differences between the defect image and the original image can be highlighted, which is conducive to the subsequent defect detection. When distinguishing between noise areas and defect areas, setting the area threshold to 200 can effectively highlight defect areas to the maximum extent, while noise areas are removed. This setting achieves the best defect detection results. However, the whole process of detection is cumbersome, mainly relying on experience and subjective setting of thresholds, and the thresholds need to be reset for other defects, resulting in poor general applicability.

4.3.2. Defect Detection Based on Improved Image Difference

(1) Background modeling

Step 1: randomly select 10 normal images of the steel ball surface, convert them into grayscale images, and apply a Gaussian smoothing filter to reduce noise.

Step 2: calculate the average of these 10 grayscale images to generate the background model image H and its frequency distribution histogram.

Step 3: Apply the adjacent frame difference method to the 10 grayscale images to obtain 9 background difference images. Then, calculate their average to obtain the background threshold image H1 and the background threshold value T1 as 17, as shown in Figures 16 and 17.

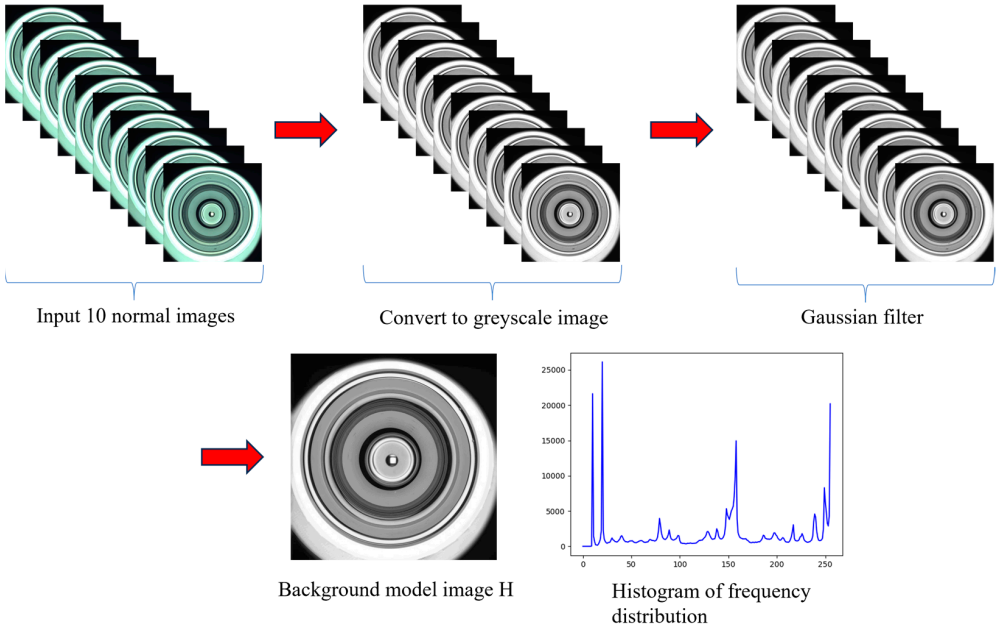


Figure 16. Flow of creating background model image.

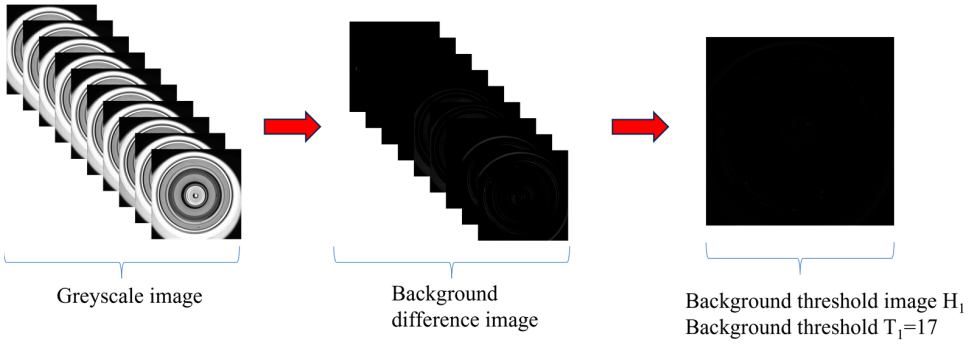


Figure 17. Flow of making background threshold image and calculating background threshold value.

(2) Defect detection

Step 1: convert the defect image to be detected into a grayscale image, and apply a Gaussian smoothing filter to obtain a low-noise grayscale image.

Step 2: calculate the difference between the defect image and the background model image H, and generate a difference image.

Step 3: by analyzing the range of the pixel values of the difference image, the max-min averaging method is used to calculate a new threshold value T2 of 76, to help distinguish between the foreground and the background.

Step 4: The background threshold T1 and the threshold T2 are added to obtain the adaptive threshold T as 93, and the binarized image is obtained by binarizing the difference image using the adaptive threshold T. Finally morphological processing is performed on the binarized image, and regions with a value of 255 are identified as defects, as shown in Figure 18.

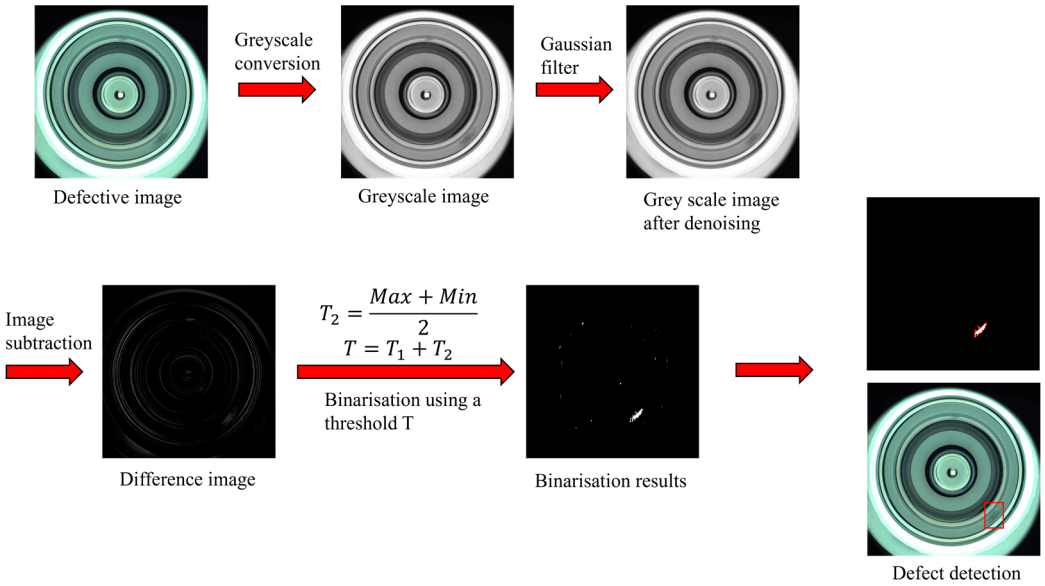


Figure 18. Flow of defect detection using improved image difference method.

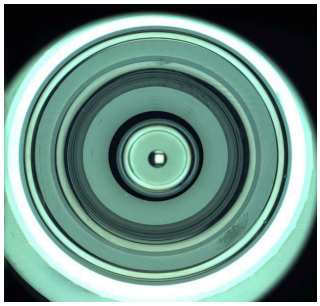
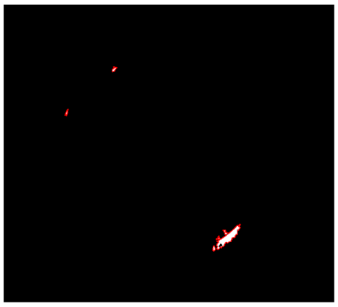
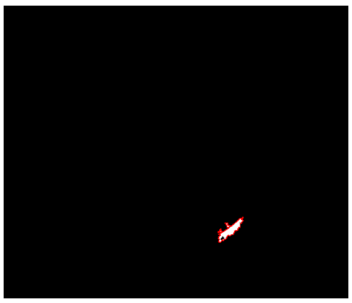
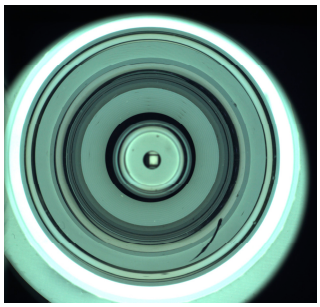
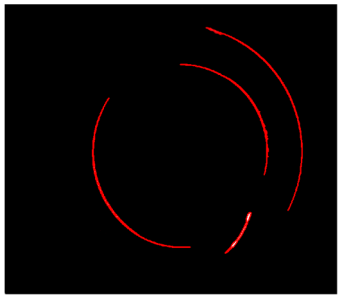
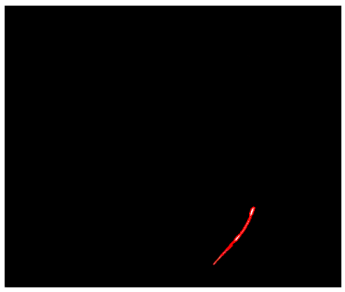
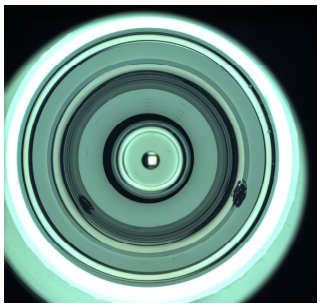
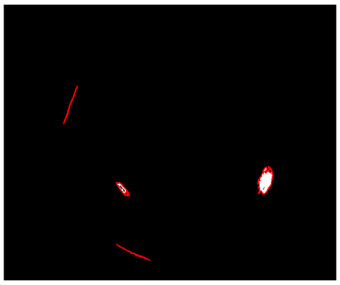
4.3.3. Analysis and Discussion

The experimental results demonstrate that the defect detection method based on improved image difference has significant advantages in detecting defects on the surface of steel balls. Compared to the traditional detection method with background difference, the improved approach achieves an increase in detection accuracy for clusters, scratches, and stains by 12%, 16%, and 14%, respectively. By introducing adaptive threshold and adjacent frame difference, the improved method effectively overcomes the subjectivity of manually setting thresholds and the lack of flexibility across different defect types seen in traditional methods. The adaptive threshold automatically adjusts based on the image's grayscale distribution, reducing noise interference and enhancing the detection precision for subtle defects. Table 4 shows the detection results for various defect types using both methods. Table 5 shows an example graph of the detection effect of the conventional method and the improved method of image difference.

Table 4. Detection results of various types of defects.

Defect Type	Sample Size	Missed Detections (Improved Method)	Detection Rate (Improved Method, %)	Missed Detections (Traditional Method)	Detection Rate (Traditional Method, %)
Cluster	50	1	98%	7	86%
Scratch	50	2	96%	10	80%
Stain	50	1	98%	8	84%

Table 5. Example of detection results.

	Sample Image	Conventional Method	Improved Method
Cluster			
Scratch			
Stain			

5. Conclusions

1. This paper introduces a novel application of the axial cone mirror's optical reflection principle to achieve a rapid and comprehensive unfolding of the three-dimensional surface of steel balls into two-dimensional images, and the complete surface image can be obtained in only two shots. Compared with the traditional unfolding method that uses rollers to capture images one by one (requiring 32 images to cover the entire surface), this method simplifies the acquisition process, significantly enhances detection efficiency, reduces equipment wear, and provides greater stability and adaptability.
2. The innovative use of adaptive thresholding and adjacent frame difference techniques in this method creates a more efficient and lightweight detection process, which realizes the lightweight of the detection process. The method can automatically adapt to different lighting conditions and defect types, reduce noise interference, and ensure stability and high-precision detection in complex environments. The accuracy rates for detecting cluster, scratch, and stain reach 98%, 96%, and 98%, respectively.
3. The methodology presented within this paper holds broad potential for practical industrial applications: the detection efficiency and applicability of the system are significantly improved by the combination of axial cone mirror expansion and improved image difference techniques. The method is not only applicable to defect detection on the surface of steel balls, but also provides a reference and technical basis for defect detection on other complex curved structures. In the future, we will leverage generative AI (e.g., GANs) and data augmentation [30,31] to create high-quality

synthetic images, enhancing system robustness and adaptability to diverse defects and complex environments.

4. This study has limitations when applied to different sizes of steel balls. Future research will consider adjusting the lens parameters and unfolding algorithms to accommodate different sizes. Integration with digital twin technology will also be explored to enable real-time monitoring and feedback in the manufacturing environment to further improve the intelligence and adaptability of the system [32].

Author Contributions: Conceptualization, C.L. and H.N.; methodology, C.L. and H.N.; software, J.Z.; hardware, C.L. and H.U.; validation, C.L., H.N. and S.L.; formal analysis, C.L. and H.N.; investigation, B.W. and S.L.; resources, C.L. and H.U.; data curation, H.N. and H.U.; writing—original draft preparation, C.L.; writing—review and editing, C.L., H.N. and J.Z.; visualization, H.N. and S.L.; supervision, S.L.; project administration, H.N.; funding acquisition, S.L. All authors have read and agreed to the published version of the manuscript.

Funding: This research was funded by A Priority Academic Program Development of Jiangsu Higher Education Institutions (PAPD), Key R&D Projects of Jiangsu Province (BE2023765), Jiangsu Province Innovation Support Program (International Science and Technology Cooperation) Project (BZ2023002), and Jiangsu Province Science and Technology Plan Special Fund (International Science and Technology Cooperation) Project (BZ2024048).

Data Availability Statement: The original contributions presented in this study are included in the article. Further inquiries can be directed to the corresponding authors.

Conflicts of Interest: The authors declare no conflicts of interest.

References

1. Cimpoesu, N.; Paleu, V.; Panaghie, C.; Roman, A.-M.; Cazac, A.M.; Cioca, L.-I.; Bejinariu, C.; Lupescu, S.C.; Axinte, M.; Popa, M.; et al. Mechanical Properties and Wear Resistance of Biodegradable ZnMgY Alloy. *Metals* **2024**, *14*, 836. [CrossRef]
2. Lu, W.; Xue, J.; Pu, W.; Chen, H.; Wang, K.; Jia, R. A Calculation Method of Bearing Balls Rotational Vectors Based on Binocular Vision Three-Dimensional Coordinates Measurement. *Sensors* **2024**, *24*, 6499. [CrossRef] [PubMed]
3. Zhou, H.; Dong, C.; Chen, F.; Cheng, L.; Wu, C.; Weng, H. A review of methods for detecting surface defects on steel balls. *Equip. Manuf. Technol.* **2018**, *10*, 7–11+47.
4. Pan, H. Establishment of Automatic Evaluation System for Surface Quality of Steel Balls and Its Application. Ph.D. Thesis, Harbin Institute of Technology, Harbin, China, 2000.
5. Tohoku Techno Arch Corporation. Non-Destructive Testing Equipment for Spheres. Japan Patent PA_2000398156, 3 April 2003.
6. Kakimoto, A. Detection of surface defects on steel ball bearings in production process using a capacitive sensor. *Measurement* **1996**, *17*, 51–57. [CrossRef]
7. Amatsuji Steel Ball Mfg. Co. Laser Type Steel Ball Appearance Inspection System. Japan Patent PA_200816442, 17 July 2008.
8. Kawasaki, K. Automatic Ultrasonic Ball Inspection Method and Apparatus. Method and Apparatus for Automatic Inspection of Balls by Ultrasonic Flaw Detection. Japan Patent PA_201012762, 10 June 2010.
9. Song, X. Surface Defect Detection of Bearing Steel Balls Based on Machine Vision. Master's Thesis, Henan University of Science and Technology, Luoyang, China, 2009.
10. Li, L. Research on the Key Technology of Rapid Detection of Highly Reflective Spherical Defects Based on Vision. Ph.D. Thesis, Tianjin University, Tianjin, China, 2013; pp. 1–5.
11. Song, Y. Research on Streak Detection Method for Highly Reflective Spherical Surface Defects. Master's Thesis, Tianjin University, Tianjin, China, 2017; pp. 1–4.
12. Papacharalampopoulos, A.; Tzimanis, K.; Sabatakakis, K.; Stavropoulos, P. Deep Quality Assessment of a Solar Reflector Based on Synthetic Data: Detecting Surficial Defects from Manufacturing and Use Phase. *Sensors* **2020**, *20*, 5481. [CrossRef] [PubMed]
13. Stavropoulos, P.; Papacharalampopoulos, A.; Petridis, D. A vision-based system for real-time defect detection: A rubber compound part case study. *Procedia CIRP* **2020**, *93*, 1230–1235. [CrossRef]
14. Li, L.; Ren, T.-M.; Feng, M. Research on surface defect identification of steel balls based on improved K-CV parameter optimization support vector machine. *Adv. Mech. Eng.* **2023**, *15*, 16878132231218586. [CrossRef]
15. Pu, H.M.; Wang, Z.; Kang, Y.H. An orthogonal clamping method and mechanism for spiral full unfolding of steel balls. *China Mech. Eng.* **2019**, *30*, 2010–2015.
16. Zhao, Y.-L.; Wang, S.-Y.; Bao, Y.-D.; Xiang, J.-Z. Design and simulation of full surface unfolding mechanism of steel ball. *J. Harbin Inst. Technol.* **2017**, *22*, 9–14. [CrossRef]
17. Xiang, J.; Zhao, C.; Zhao, Y.; Tan, Y.; Jiang, C.; Deng, J.; Zhang, S.; Hu, D.; Yan, Z. Effective area analysis of image-based steel ball defect detection. *J. Harbin Inst. Technol.* **2017**, *22*, 65–69. [CrossRef]

18. Kawabata, O.; Ukita, H. Investigation of appearance inspection method for all surfaces of steel balls. In Proceedings of the Dynamic Image Processing Application Workshop (DIA2023), Toyama, Japan, 3–4 March 2023; pp. 66–70.
19. Garcia-Garcia, B.; Bouwmans, T.; Silva, A.J.R. Background subtraction in real applications: Challenges, current models and future directions. *Comput. Sci. Rev.* **2020**, *35*, 100204. [CrossRef]
20. Cermelli, F.; Mancini, M.; Bulo, S.R.; Ricci, E.; Caputo, B. Modeling the background for incremental learning in semantic segmentation. In Proceedings of the IEEE/CVF Conference on Computer Vision and Pattern Recognition, Seattle, WA, USA, 13–19 June 2020; pp. 9233–9242.
21. Chen, J.; Wu, Q.; Liu, D.; Xu, T. Foreground-background imbalance problem in deep object detectors: A review. In Proceedings of the 2020 IEEE Conference on Multimedia Information Processing and Retrieval (MIPR), Shenzhen, China, 6–8 August 2020; IEEE: Piscataway, NJ, USA, 2020; pp. 285–290.
22. Meier, T.; Ngan, K.N. Automatic segmentation of moving objects for video object plane generation. *IEEE Trans. Circuits Syst. Video Technol.* **1998**, *8*, 525–538. [CrossRef]
23. Liu, J.; Huang, Y.; Zhang, M.; Zhou, S.; Nie, C.; Li, M.; Zhang, L. Detecting Steam Leakage in Nuclear Power Systems Based on the Improved Background Subtraction Method. *Processes* **2024**, *12*, 1538. [CrossRef]
24. Soeleman, M.A.; Nurhindarto, A.; Muslih, M.; Karis, W.M.; Muljono, M.; Zami, F.A.; Pramunendar, R.A. Adaptive threshold for moving objects detection using gaussian mixture model. *TELKOMNIKA Telecommun. Comput. Electron. Control* **2020**, *18*, 1122–1129. [CrossRef]
25. Barron, J.T.A. Generalization of Otsu's method and minimum error thresholding. In *Computer Vision—Proceedings of the ECCV 2020 16th European Conference, Glasgow, UK, 23–28 August 2020*; Proceedings, Part V 16; Springer International Publishing: Cham, Switzerland, 2014; pp. 455–470.
26. Laiginhas, R.; Cabral, D.; Falcão, M. Evaluation of the different thresholding strategies for quantifying choriocapillaris using optical coherence tomography angiography. *Quant. Imaging Med. Surg.* **2020**, *10*, 1994–2005. [CrossRef] [PubMed]
27. Jiang, M.-H.; Fu, L.-H.; Wang, Z.; Song, Y.-H. A new method for specular curved surface defect inspection-based on reflected pattern integrity. *J. Meas. Sci. Instrum.* **2016**, *7*, 221–228. [CrossRef]
28. Liu, Q.; Zhang, J.; Huang, J. Detection and classification of steel ball surface defects based on machine vision. *Bearing* **2013**, *10*, 44–48. [CrossRef]
29. Qian, X.; Gan, X.; Liu, X.; Lu, Y.; Zhang, X.; Ju, A.; Ma, X. Neighbourhood denoising and image differencing for detecting surface defects in carbon fibre tow spreading. *J. Donghua Univ. (Nat. Sci. Ed.)* **2024**, 1–6. [CrossRef]
30. Stavropoulos, P.; Papacharalampopoulos, A.; Sabatakakis, K. Online Quality Inspection Approach for Submerged Arc Welding (SAW) by Utilizing IR-RGB Multimodal Monitoring and Deep Learning. In *Flexible Automation and Intelligent Manufacturing: The Human-Data-Technology Nexus*; Kim, K.-Y., Monplaisir, L., Rickli, J., Eds.; Springer International Publishing: Cham, Switzerland, 2023; pp. 160–169.
31. Lian, J.; Jia, W.; Zareapoor, M.; Zheng, Y.; Luo, R.; Jain, D.K.; Kumar, N. Deep-Learning-Based Small Surface Defect Detection via an Exaggerated Local Variation-Based Generative Adversarial Network. *IEEE Trans. Ind. Inform.* **2020**, *16*, 1343–1351. [CrossRef]
32. Stavropoulos, P.; Papacharalampopoulos, A.; Sabatakakis, K.; Mourtzis, D. Metamodelling of Manufacturing Processes and Automation Workflows towards Designing and Operating Digital Twins. *Appl. Sci.* **2023**, *13*, 1945. [CrossRef]

Disclaimer/Publisher's Note: The statements, opinions and data contained in all publications are solely those of the individual author(s) and contributor(s) and not of MDPI and/or the editor(s). MDPI and/or the editor(s) disclaim responsibility for any injury to people or property resulting from any ideas, methods, instructions or products referred to in the content.